PERGAMON

International Journal of Multiphase Flow 28 (2002) 1763–1785

International Journal of Multiphase Flow

www.elsevier.com/locate/ijmulflow

Numerical modeling of large-scale bubble plumes accounting for mass transfer effects

Gustavo C. Buscaglia [a,*], Fabián A. Bombardelli [b], Marcelo H. García [b]

[a] *Centro Atómico Bariloche and Instituto Balseiro, 8400 Bariloche, Argentina*
[b] *Ven Te Chow Hydrosystems Laboratory, Department of Civil and Environmental Engineering, University of Illinois at Urbana-Champaign, Urbana IL 61801, USA*

Received 16 October 2001; received in revised form 26 June 2002

Dedicated to the innocent victims of September 11, 2001. Rest in peace

Abstract

A mathematical model for dilute bubble plumes is derived from the two-fluid model equations. This is coupled to a mass transfer model to get a closed CFD formulation. The mass transfer equations used are the same as those implemented in the 1D model proposed, so as to get a CFD formulation and a 1D integral formulation that are fully consistent. In fact, the 1D model can be rigorously derived from the CFD one. The mathematical derivation is detailed pointing out the approximations involved.

Results of both models for typical conditions of isolated aeration plumes in deep wastewater reservoirs are presented. Good agreement is reported between them, emphasizing on the most relevant variables such as gas dissolution rates, gas holdup, liquid's velocity and bubbles' radius. Furthermore, entrainment rates evaluated from the CFD results are shown to lie within the experimental range. Finally, CFD-based assessment of the approximations involved in the 1D model proves them to hold within a few percents of relative accuracy. A solid basis for applying CFD models to aeration plumes, as natural extensions of the popular integral models, emerges from the investigation.

Keywords: Two-phase flow; Bubble plumes; Two-fluid equations; Integral models

* Corresponding author.
E-mail address: gustavo@cab.cnea.gov.ar (G.C. Buscaglia).

0301-9322/02/$ - see front matter
PII: S0301-9322(02)00075-7

1. Introduction

Air-bubble plumes have numerous applications such as pneumatic breakwaters, antifreeze measures, silt curtains, and barriers to contain density intrusions or oil spills (Ashton, 1978; Bulson, 1968; Ditmars and Cederwall, 1974; Taylor, 1955). For deep water bodies (lakes, reservoirs) injection of air-bubbles is often used for destratification of the water volume (Schladow, 1992; Asaeda and Imberger, 1993; Lemckert and Imberger, 1993). In wastewater treatment aeration with bubble plumes has been employed for about a century (Joint Task Force WPCF-ASCE, 1988), however its use in deep reservoirs containing biochemically active water is an emerging application. The construction of large wastewater reservoirs is being motivated by environmental concerns. The idea is to provide storage for combined sewage and stormwater during big storms, so that water treatment plants can operate in batch mode. This is an important problem in large metropolitan areas such as Chicago, Illinois.

Power efficiency in aeration devices for deep water bodies is essential due to the high injection pressure needed. Design optimization with sound scientific tools is thus in order, and numerical modeling is without doubt one of the key tools in all fields of engineering. In plume modeling simulation codes have mostly used the transversally integrated equations (McDougall, 1978; Milgram, 1983; Schladow, 1992; Asaeda and Imberger, 1993; Lemckert and Imberger, 1993; Wüest et al., 1992), based on a self-similarity assumption and the well-known entrainment hypothesis (see, e.g., Turner, 1986). The problem is thus reduced to just one spatial dimension, at the cost of introducing some heuristic coefficients that must be obtained from experiments.

A transversally integrated model (frequently referred to as *integral model*) that accounts for most of the physical and chemical processes related to aeration of reservoirs was introduced by Wüest et al. (1992) to help in the design of lake restoration systems. The aim of the present article is to extend that model in a systematic way to two-fluid flow modeling and computational fluid dynamics (CFD). An improved formulation results which has less empirical coefficients and can deal with arbitrary geometries. Moreover, wastewater reservoir aeration involves the simultaneous operation of many bubble plumes. While integral models assume the plume to be isolated, CFD formulations are the appropriate tool to study plume–plume, plume–boundary and plume–crossflow interactions.

The two-fluid model proposed here is based on the general theory of multiphase flows (Drew and Passman, 1998) and has three main components:

- A hydrodynamical component that considers the main physical processes in a free dilute bubbly flow, i.e., the increase in effective buoyancy by bubbles, the non-zero slip velocity between the gas and the liquid, and the turbulent dispersion of bubbles. In two-fluid-model terminology, the interfacial forces considered are buoyancy, drag and turbulent dispersion. Away from walls these are generally the most important forces in dilute bubbly flows (see, e.g., Loth (2000) for a recent review on the subject). The mass conservation equation for the gas is rewritten in terms of a *terminal velocity* and an *effective dispersion coefficient* as done by Moraga et al. (submitted for publication). The former is fitted from experimental data as done by Wüest et al. (1992), while several options are available for the latter, as those proposed by Carrica et al. (1998), by López de Bertodano (1998) and by Loth (2001). The resulting model is basically the same that recently allowed Sokolichin and Eigenberger (1999) to reproduce dynamical structures ob-

served in a locally aerated flat bubble column with remarkable success, a problem that has challenged the simulation capabilities of much more elaborate two-fluid models such as that of Mudde and Simonin (1999).
- A mass transfer component that considers oxygen and nitrogen dissolution from the bubbles and was taken from Wüest et al. (1992).
- A liquid chemistry component that incorporates a basic water-quality model taken from the book by Chapra (1997). The variables are dissolved oxygen concentration, dissolved nitrogen concentration, and the biochemical oxygen demand that encompasses all oxygen-consuming processes.

Integral models are extensively used in environmental fluid dynamics, mainly because they are simple, robust and physically based. Since our intention is to complement those models with the proposed CFD-based one, a significant portion of the presentation is devoted to a comparative assessment in which the same problems are solved with both strategies. The comparison yields good agreement in the cases considered, resulting in a fully consistent picture of 1D and CFD models. This is complemented with comparisons of CFD results for the entrainment rate with available data and with a CFD-based assessment of the approximations inherent in integral models.

The organization of the paper is as follows: In Section 2 a mathematical model for dilute bubbly flows is described and justified in which the mass exchange between liquid and gas, together with a basic water-quality model, are incorporated. Section 3 describes the numerical treatment of the model equations in the CFD code. In Section 4 the relation between the proposed model and the integral model of Wüest et al. (1992) is shown. Section 5 contains numerical results comparing the predictions of both models for isolated plumes at conditions typical of deep wastewater reservoirs. Finally, the most relevant conclusions are drawn in Section 6.

2. Mathematical model

2.1. Two-fluid model and dynamical equations

The two-fluid model can be obtained by ensemble averaging the exact conservation equations for each phase in a multiphase flow, as discussed by Drew and Passman (1998). Let $X_k(x,t;v)$ be the *component indicator function*, which for a given realization v of the flow takes the value one if phase k is present at point x at time t, and takes the value zero otherwise. The following averaged quantities are needed to write down the equations:

- $\alpha_k = \overline{X}_k$, is the so-called volume fraction of phase k but is, in fact, the *probability* of phase k.
- The averaged density and velocity of phase k are defined by

$$\overline{\rho}_k = \frac{\overline{X_k \rho}}{\alpha_k}; \quad \overline{u}_k = \frac{\overline{X_k \rho u}}{\alpha_k \overline{\rho}_k} \tag{1}$$

- The pressure, on the other hand, is not mass averaged,

$$\overline{p}_k = \frac{\overline{X_k p}}{\alpha_k} \tag{2}$$

We neglect pressure differences between the phases ($\overline{p}_k = \overline{p}$, $\forall k$) and the shear stresses at the interphase. We denote by Γ_k the interphase mass transfer rate ($\sum_k \Gamma_k = 0$) and neglect the momentum transfer arising from mass transfer between the phases. One ends up with the following averaged equations for phase k:

$$\frac{\partial \alpha_k \overline{\rho}_k}{\partial t} + \operatorname{div}(\alpha_k \overline{\rho}_k \overline{u}_k) = \Gamma_k \tag{3}$$

$$\frac{\partial \alpha_k \overline{\rho}_k \overline{u}_k}{\partial t} + \operatorname{div}(\alpha_k \overline{\rho}_k \overline{u}_k \otimes \overline{u}_k) + \alpha_k \nabla \overline{p} = \operatorname{div}(\alpha_k \overline{T}_k) - \alpha_k \overline{\rho}_k g \mathbf{k} + M'_k \tag{4}$$

where the effective stress $\overline{T}_k$ contains both the averaged deviatoric stresses of phase k and the fluctuation stress tensor that arises from the inertia term along the averaging process. Here $\mathbf{k}$ is the upwards vertical unit vector and g is the acceleration of gravity. The interfacial forces such as drag, lift, etc. are contained in M'_k, with $\sum_k M'_k = 0$.

The averaged equations implemented in our code consider a liquid phase ($k = \ell$) and a gaseous phase ($k = \mathrm{g}$). We will make use of the *mixture* equations, which are obtained by adding up the balance equations of the individual phases. Let us define the mixture quantities as

$$\rho_\mathrm{m} = \alpha_\ell \overline{\rho}_\ell + \alpha_\mathrm{g} \overline{\rho}_\mathrm{g} \tag{5}$$

$$\rho_\mathrm{m} u_\mathrm{m} = \alpha_\ell \overline{\rho}_\ell u_\ell + \alpha_\mathrm{g} \overline{\rho}_\mathrm{g} \overline{u}_\mathrm{g} \tag{6}$$

$$T_\mathrm{m} = \alpha_\ell \overline{T}_\ell + \alpha_\mathrm{g} \overline{T}_\mathrm{g} \tag{7}$$

$$p_\mathrm{m} = \overline{p} \tag{8}$$

Then, from (3) and (4) it follows that

$$\frac{\partial \rho_\mathrm{m}}{\partial t} + \operatorname{div}(\rho_\mathrm{m} u_\mathrm{m}) = 0 \tag{9}$$

$$\frac{\partial \rho_\mathrm{m} u_\mathrm{m}}{\partial t} + \operatorname{div}(\rho_\mathrm{m} u_\mathrm{m} \otimes u_\mathrm{m}) + \nabla p_\mathrm{m} = \operatorname{div} T_\mathrm{m} - \rho_\mathrm{m} g \mathbf{k} - \operatorname{div}\left[\sum_k \alpha_k \overline{\rho}_k (\overline{u}_k - u_\mathrm{m}) \otimes (\overline{u}_k - u_\mathrm{m}) \right] \tag{10}$$

Let us define the relative velocity between the phases as $u_\mathrm{r} = \overline{u}_\mathrm{g} - \overline{u}_\ell$, so that the summation in the last term of (10) satisfies

$$\sum_k \alpha_k \overline{\rho}_k (\overline{u}_k - u_\mathrm{m}) \otimes (\overline{u}_k - u_\mathrm{m}) = \alpha_\mathrm{g} \overline{\rho}_\mathrm{g} \left(1 - \frac{\alpha_\mathrm{g} \overline{\rho}_\mathrm{g}}{\rho_\mathrm{m}} \right) u_\mathrm{r} \otimes u_\mathrm{r} \tag{11}$$

This term is neglected in the following since both α_g and $\overline{\rho}_\mathrm{g}/\rho_\mathrm{m}$ are assumed to be much smaller than unity, while u_r and u_m are of the same order.

Notice that

$$\rho_\mathrm{m} = \overline{\rho}_\ell - \alpha_\mathrm{g} (\overline{\rho}_\ell - \overline{\rho}_\mathrm{g}) \tag{12}$$

so that $\rho_\mathrm{m} - \overline{\rho}_\ell \approx -\alpha_\mathrm{g} \overline{\rho}_\ell$. Assuming the liquid phase to be incompressible, with reference density ρ_0 (i.e., $\rho_0 = \overline{\rho}_\ell$), we can now adopt the Boussinesq approximation replacing ρ_m by ρ_0 in all terms but the gravity one. This approximation is routinely applied in thermal problems with temper-

ature differences as high as 20 °C (in water), so that one can expect it to hold for values of α_g leading to the same magnitude of density change, i.e., $\alpha_g < 10^{-2}$.

The resulting balance equations are, thus,

$$\operatorname{div} u_m = 0 \tag{13}$$

$$\rho_0 \frac{\partial u_m}{\partial t} + \rho_0 \operatorname{div}(u_m \otimes u_m) + \nabla p_m = \operatorname{div} T_m - \rho_m g \mathbf{k} \tag{14}$$

which are indeed very simple but as shown above follow from the two-fluid model under reasonable hypotheses. The incompressibility condition for u_m greatly simplifies the mathematical structure of the problem, restoring the classical Navier–Stokes structure. This is a significant advantage with respect to (9) and (10), which contain derivatives of ρ_m (and thus of α_g) resulting in a strong coupling with the mass balance equation for the gas. Well-posedness results for the coupled system (i.e., without the quasi-incompressibility, Boussinesq approximation) do not exist, moreover in simplified one-dimensional cases it can be shown that the system is ill-posed, at least conditionally (see Drew and Passman, 1998; Song and Ishii, 2001).

We stress that up to this point only an ensemble average so as to homogenize the phases and define phase-related average quantities such as the volume fraction α_k, has been performed. This does not necessarily imply that all turbulent fluctuations have been averaged and we are dealing with a Reynolds-averaged Navier–Stokes (RANS) formulation. This is best understood in terms of volume averages such as those discussed by Ganesan and Poirier (1990) and Ni and Beckermann (1991). It is immediate that to get the average equations for each phase, (3) and (4), only the spatial scales of the order of the bubble-to-bubble spacing L_{bb} (and smaller) need to be averaged. If there exist turbulence scales much larger than L_{bb}, as generally occurs in bubble plumes at environmental scale, these can be kept to be modeled later (or solved directly). In terms of temporal averages, on the other hand, the averaging window only needs to be greater than the typical gas/liquid intermittence time scale, which may be much smaller than the large-eddy time scale.

We thus assume that T_m in (14) contains just the contributions of the laminar deviatoric stresses of each phase and of the turbulent fluctuations at scales smaller than or equal to some specified length L_c which is greater than L_{bb}. This "hierarchical" averaging approach appears intuitive when there exist turbulent length scales much larger than L_{bb} and is discussed to some extent by Besnard and Harlow (1988). It underlies some classical approaches to multiphase flow formulations (see, e.g., the book by Soo (1990)) and one can easily conceive a "conditional" ensemble-averaging procedure that leads to the same result.

By contrast, the work of Drew and Passman (1998) and of Carrica et al. (1998, 1999) assumes that the ensemble-averaging process encompasses all fluctuating scales, so that a RANS formulation is obtained after a single averaging step. López de Bertodano (1998) argues that otherwise a second averaging procedure is needed to get a RANS formulation, which would lead to a more involved momentum equation for each phase.

In dilute bubbly flows the main difference between the two approaches concerns the mass balance equation for the gas. Let us denote by $\langle\cdot\rangle$ the Reynolds averaging operator of the large turbulent scales that persist after the application of the operator $\overline{(\cdot)}$ because their length scale is greater than L_c. Let us denote by m_g the mass concentration of gas, defined as the mass of gas per

unit volume of the mixture, $m_g = \alpha_g \bar{\rho}_g$. The Reynolds-averaged mass balance equation for the gas is thus,

$$\frac{\partial}{\partial t}\langle m_g \rangle + \mathrm{div}(\langle m_g \rangle \langle \overline{u}_g \rangle) = \langle \Gamma_g \rangle - \mathrm{div}(\langle m_g \overline{u}_g \rangle - \langle m_g \rangle \langle \overline{u}_g \rangle) \tag{15}$$

This equation is also obtained if $\langle \cdot \rangle$ is a LES filter instead of a Reynolds average. The simplest closure assumption is a gradient approximation with a gas diffusivity tensor $\mathscr{D}_g$, which leads to

$$\frac{\partial}{\partial t}\langle m_g \rangle + \mathrm{div}(\langle m_g \rangle \langle \overline{u}_g \rangle) = \langle \Gamma_g \rangle + \mathrm{div}(\mathscr{D}_g \nabla \langle m_g \rangle) \tag{16}$$

We insist in that the last term of this equation only models the gas dispersion due to the turbulent scales larger than L_c, which persist after applying the $\overline{(\cdot)}$ operator. In particular, for the single-average approach the last term is non-existent. In any case, the dispersion by turbulence at scales that *are* averaged by the $\overline{(\cdot)}$ appears in the *momentum* equation for the gas as a *turbulent dispersion force* (or as a *drift velocity* correction in the formulations of Simonin and Viollet (1988), Viollet and Simonin (1994) and Mudde and Simonin (1999)).

Moraga et al. (submitted for publication) recently performed an assessment of models for the turbulent dispersion. They pointed out that, in fact, when the dominant forces are drag, buoyancy and turbulent dispersion both approaches (with single or double average) are equivalent. Remarkably, DNS results only exist for this drag–turbulence dominated case (Druzhinin and Elghobashi, 1998), and experimental data accurate enough to distinguish between the two approaches in problems with significant virtual-mass effects are not available.

From the numerical viewpoint, if turbulent dispersion is dealt with in the mass equation for the gas, as in (16), it is quite simple to treat it in a backward-Euler manner, which is much more stable than the usual forward-Euler treatment. This is also feasible in the single-average approach, but much more involved (Kunz et al., 1998).

Since it is numerically convenient, equivalent to the single-average approach in all cases for which reliable data exist, and physically sound, we have adopted the double-average approach in this work. Except very close to the diffuser, the bubbles Stokes numbers in environmental-scale bubble plumes are extremely small, so that one would expect no significant differences between both approaches in our cases of interest.

The system of equations we have introduced so far consists of (13), (14) and (16), supplemented by the algebraic relation (12). We still need to introduce a turbulent closure, and equations for $\langle \overline{u}_g \rangle$, Γ_g and $\mathscr{D}_g$. There exist many alternatives to do this. Our approach here is to produce a CFD formulation that mimics the integral model of Wüest et al. (1992), so as to compare the two codes. Other possibilities are pointed out along the presentation, but their assessment is left for future work.

2.2. Adopted CFD formulation

Standard Reynolds averaging is applied to the mixture equations (13) and (14), adopting a k–ϵ model for the turbulence closure. The mixture stress tensor T_m is assumed much smaller than the Reynolds stresses arising from the second averaging process, and is neglected. The pressure is

modified as $\hat{p}_m = p_m + (2/3)k$ to account for the spherical part of the Reynolds stresses. We omit hereafter all the averaging operators to simplify the notation. The final equations are

$$\operatorname{div} u_m = 0 \tag{17}$$

$$\rho_0 \frac{\partial u_m}{\partial t} + \rho_0 \operatorname{div}(u_m \otimes u_m) + \nabla \hat{p}_m = \operatorname{div}[\mu_T(\nabla u_m + \nabla^T u_m)] - \rho_m g \mathbf{k} \tag{18}$$

$$\mu_T = \rho_0 C_\mu \frac{k^2}{\epsilon} \tag{19}$$

where $C_\mu = 0.09$. The equations for k and ϵ, together with the treatment of wall laws, correspond to the standard model (see, e.g., the book by Wilcox (1998); our implementation is presented in Lew et al. (2001)). No corrections for buoyancy effects or bubble-induced turbulence are performed.

This certainly deserves a comment. Several corrections to the k–ϵ equations to account for the effect of bubbles have been proposed. A popular one is due to Sato et al. (1981), who add $1.2\rho_0 r_b \alpha_g |u_r|$ to the eddy viscosity, where r_b is the bubble radius. Typical values obtained for μ_T are above 10 Pa s, while usual values are $r_b = 2 \times 10^{-3}$ m, $|u_r| = 0.3$ m/s and $\alpha_g < 10^{-2}$. The correction would thus be smaller than 10^{-2} Pa s, which can clearly be neglected.

Mudde and Simonin (1999) applied a k–ϵ model with quite elaborate corrections proposed by Viollet and Simonin (1994) to simulate the plume-wandering experiments of Becker et al. (1994). Only after adding virtual-mass effects did they get agreement with the experimental data. However, the 3D simulations of Sokolichin and Eigenberger (1999) and of Borchers et al. (1999) with the *standard* k–ϵ model (and a constant bubble-slip velocity!) show excellent agreement. Similar agreement was also obtained by Pfleger et al. (1999) with again the standard model but a drag law to calculate bubble-slip velocity. Smith (1998), on the other hand, concludes that the corrections of Viollet and Simonin (1994) do bring some improvement, while those of Malin and Spalding (1984) lead to incorrect results.

Overall one observes that, *at least for bubble-plume modeling*, the two-phase turbulence closure controversy is far from settled. It is thus natural to start with the simplest model, as done by several other authors such as Grevet et al. (1982), Woo et al. (1990), Joo and Guthrie (1992), Hua and Wang (2000) and Morchain et al. (2000).

2.3. Gas-phase model

The gas-phase model of Wüest et al. (1992) is quite simple. No bubble coalescence or breakup is accounted for, so that the (averaged) number of bubbles per unit volume N_b satisfies

$$\frac{\partial N_b}{\partial t} + \operatorname{div}(N_b u_g) = \operatorname{div}(\mathscr{D}_g \nabla N_b) \tag{20}$$

and the bubbles are assumed to have a unimodal size distribution. Breakup and coalescence terms that can be added on the right-hand side of this equation have been developed by Millies et al. (1996) and later simplified and validated against more than 2000 experimental data by Millies and Mewes (1999). Bubble sizes are expected to be "sheared down" near the diffuser (Hinze, 1955), with little coalescence farther above it, as observed by Tekeli and Maxwell (1978). This will however be the subject of future research.

The model also assumes a bubble-slip velocity that only depends on the bubble radius, i.e.,

$$u_g = u_m + w_b(r_b)\mathbf{k}, \quad \text{with } w_b = \begin{cases} 4474\ \text{m/s} \times r_b^{1.357} & \text{if } 0 \leqslant r_b \leqslant 7 \times 10^{-4}\ \text{m} \\ 0.23\ \text{m/s} & \text{if } 7 \times 10^{-4} < r_b \leqslant 5.1 \times 10^{-3}\ \text{m} \\ 4.202\ \text{m/s} \times r_b^{0.547} & \text{if } r_b > 5.1 \times 10^{-3}\ \text{m} \end{cases} \tag{21}$$

where r_b is expressed in meters. The velocity law is a fit to data presented by Haberman and Morton (1954), a thorough presentation of terminal velocities of bubbles in water can be found in the book by Clift et al. (1978). The alternative is to solve a momentum balance equation for the bubbles, accounting for the forces exerted by the liquid such as drag, lift, virtual mass, etc. This is not expected to produce large differences in the cases analyzed herein because plumes are free shear flows, with little dynamic effects on the pressure. The lift force could have an effect, inducing non-vertical slip velocities, but the net effect of usual models of the lift force (see, e.g., Drew and Passman, 1998) would be similar to that of turbulent dispersion.

Turning now to the dispersion coefficient $\mathscr{D}_g$, we have adopted the isotropic model (so that $\mathscr{D}_g$ becomes a scalar) proposed by Carrica et al. (1998),

$$\mathscr{D}_g = \frac{\mu_T}{\rho_0 Sc_g} \tag{22}$$

with the Schmidt number for the gas Sc_g taken equal to one. Moraga et al. (submitted for publication) recommend 0.83 for very small bubbles (small Stokes numbers), but it is expected to increase for larger ones. More sophisticated models for the dispersion coefficient are discussed by Loth (2000, 2001), but an assessment of their consequences in plume modeling is left for future work. For large-scale plumes the bubble-slip velocity $|u_r|$ far above the diffuser may be significant as compared to the characteristic eddy velocity $|u_e|$. This causes the bubbles to leave the fluid eddies because of the relative motion and not because the eddy itself breaks apart. This phenomenon, referred to as *crossing-trajectory effect*, was analyzed by Wells and Stock (1983), Wang and Stock (1993) and Stock (1996), and leads to a decreased and anisotropic turbulent dispersion.

Finally, the gas concentration equations are introduced. They are elementary modifications of (16) to account for air as a binary mixture.

We consider the gas to consist basically of two species, gaseous nitrogen and gaseous oxygen, and we introduce the molar concentrations C_N and C_O, defined as the number of moles of each gas *per unit volume of mixture*. The following relations are elementary ($\mathscr{R}$ is the universal gas constant, 8.314 J/mol K, T_g is the absolute gas temperature, assumed known, $\mathscr{M}_N$ and $\mathscr{M}_O$ refer to the molecular weights of N_2, 28 kg/kmol, and O_2, 32 kg/kmol)

$$\alpha_g = \frac{\mathscr{R} T_g (C_N + C_O)}{p_g} \tag{23}$$

$$\rho_g = \frac{C_N \mathscr{M}_N + C_O \mathscr{M}_O}{\alpha_g} \tag{24}$$

The pressure of the gas is assumed to obey $\rho_0 g(H + H_a - z)$, where H is the maximum depth, H_a the atmospheric head, and z the vertical coordinate measured from the point of maximum depth. Surface tension effects are thus not modeled in the present version, but could easily be added. It is

unlikely that non-hydrostatic effects be significant in any environmental plume, but would not represent a major difficulty either.

Mass balance of each species thus decomposes (16) into

$$\frac{\partial C_{\mathrm{O}}}{\partial t} + \operatorname{div}(C_{\mathrm{O}} u_{\mathrm{g}}) = \mathscr{S}_{\mathrm{O}} + \operatorname{div}\left(\frac{\mu_{\mathrm{T}}}{\rho_0 Sc_{\mathrm{g}}} \nabla C_{\mathrm{O}} \right) \tag{25}$$

$$\frac{\partial C_{\mathrm{N}}}{\partial t} + \operatorname{div}(C_{\mathrm{N}} u_{\mathrm{g}}) = \mathscr{S}_{\mathrm{N}} + \operatorname{div}\left(\frac{\mu_{\mathrm{T}}}{\rho_0 Sc_{\mathrm{g}}} \nabla C_{\mathrm{N}} \right) \tag{26}$$

where $\mathscr{S}_{\mathrm{O}}$ and $\mathscr{S}_{\mathrm{N}}$ are mass source terms that arise from the chemical interaction (dissolution) of the gas in the surrounding fluid, to be discussed in the next subsection. Notice that $\mathscr{M}_{\mathrm{O}}\mathscr{S}_{\mathrm{O}} + \mathscr{M}_{\mathrm{N}}\mathscr{S}_{\mathrm{N}} = \langle \Gamma_{\mathrm{g}} \rangle$ and $\mathscr{M}_{\mathrm{O}}\mathscr{C}_{\mathrm{O}} + \mathscr{M}_{\mathrm{N}}\mathscr{C}_{\mathrm{N}} = \langle m_{\mathrm{g}} \rangle$, so that (16) is recovered by adding up (25) and (26), each multiplied by the corresponding molecular weight.

From N_{b}, C_{O} and C_{N} the bubble volume v_{b} is readily obtained,

$$v_{\mathrm{b}} = \frac{(C_{\mathrm{O}} + C_{\mathrm{N}})\mathscr{R}T_{\mathrm{g}}}{p_{\mathrm{g}} N_{\mathrm{b}}} \tag{27}$$

2.4. Liquid chemistry model

We describe here the water chemistry model used by Wüest et al. (1992), slightly modified so as to account for oxygen demand. The water chemical variables are the molar concentrations of dissolved oxygen, C_{dO}, and dissolved nitrogen, C_{dN}, together with the biochemical oxygen demand modeled as a scalar field, L. The units of C_{dO} and C_{dN} are mol per cubic meter of mixture, which is about the same as mol per cubic meter of liquid since the gas fraction is assumed small. The units of L are kg per cubic meter of mixture.

The balance equations are

$$\frac{\partial C_{\mathrm{dO}}}{\partial t} + u_\ell \cdot \nabla C_{\mathrm{dO}} = \mathscr{S}_{\mathrm{dO}} + \operatorname{div}\left(\frac{\mu_{\mathrm{T}}}{\rho_0 Sc_\ell} \nabla C_{\mathrm{dO}} \right) \tag{28}$$

$$\frac{\partial C_{\mathrm{dN}}}{\partial t} + u_\ell \cdot \nabla C_{\mathrm{dN}} = \mathscr{S}_{\mathrm{dN}} + \operatorname{div}\left(\frac{\mu_{\mathrm{T}}}{\rho_0 Sc_\ell} \nabla C_{\mathrm{dN}} \right) \tag{29}$$

$$\frac{\partial L}{\partial t} + u_\ell \cdot \nabla L = -(K_1 + K_3)L + \operatorname{div}\left(\frac{\mu_{\mathrm{T}}}{\rho_0 Sc_\ell} \nabla L \right) \tag{30}$$

where u_ℓ, the mean liquid velocity, is assumed equal to the mixture velocity u_{m} and just one turbulent Schmidt number for the liquid's chemistry has been used, Sc_ℓ (usually 0.83). The constants K_1 and K_3 are given by Chapra (1997). We have taken $K_1 = 3.47 \times 10^{-6}\ \mathrm{s}^{-1}$, $K_3 = 6.94 \times 10^{-6}\ \mathrm{s}^{-1}$.

The source of dissolved oxygen depends on the exchange with gaseous oxygen, $\mathscr{S}_{\mathrm{O}}$, and on the biochemical demand L following

$$\mathscr{S}_{\mathrm{dO}} = -\mathscr{S}_{\mathrm{O}} - \frac{K_1}{\mathscr{M}_{\mathrm{O}}} L \tag{31}$$

while for nitrogen just the gas–liquid exchange was considered, i.e.,

$$\mathscr{S}_{\mathrm{dN}} = -\mathscr{S}_{\mathrm{N}} \tag{32}$$

The gaseous exchange is here discussed for oxygen, the case of nitrogen being analogous. It is clear that the net exchange is $\mathscr{S}_{\mathrm{O}} = \mathscr{A}_{\mathrm{b}} F_{\mathrm{O}}$, where $\mathscr{A}_{\mathrm{b}}$ is the interfacial area density and F_{O} the mean molar surface flux of oxygen, defined positive when flowing from liquid to gas. A typical model for F_{O} is $F_{\mathrm{O}} = h_{\mathrm{m}}(C_{\mathrm{dO}} - C_{\mathrm{dO,I}})$, where h_{m} is the mass transfer coefficient and $C_{\mathrm{dO,I}}$ is the concentration of dissolved oxygen at the gas–liquid interface. Assuming local thermodynamic equilibrium at the interface, $C_{\mathrm{dO,I}} = K_{\mathrm{O}} p_{\mathrm{O}}$, with K_{O} the Henry's constant and p_{O} the partial pressure of oxygen inside the bubble, $p_{\mathrm{O}} = p_{\mathrm{g}} C_{\mathrm{O}}/(C_{\mathrm{O}} + C_{\mathrm{N}})$. The assumption that the gas inside the bubble has uniform oxygen concentration is implicit in the previous model.

Assuming bubbles to be spherical and of uniform size at each point, $\mathscr{A}_{\mathrm{b}} = (36\pi)^{1/3} v_{\mathrm{b}}^{2/3} N_{\mathrm{b}}$, and from (27) $N_{\mathrm{b}} = (C_{\mathrm{O}} + C_{\mathrm{N}})\mathscr{R} T_{\mathrm{g}}/(p_{\mathrm{g}} v_{\mathrm{b}})$, so that $\mathscr{A}_{\mathrm{b}} = (36\pi/v_{\mathrm{b}})^{1/3} \mathscr{R} T_{\mathrm{g}}(C_{\mathrm{O}} + C_{\mathrm{N}})/p_{\mathrm{g}}$. The identity, again for spheres, $(36\pi/v_{\mathrm{b}})^{1/3} = 3/r_{\mathrm{b}}$ leads to the final expressions, for oxygen and nitrogen,

$$\mathscr{S}_{\mathrm{O}} = \frac{3\mathscr{R} T_{\mathrm{g}}(C_{\mathrm{O}} + C_{\mathrm{N}}) h_{\mathrm{m}}}{p_{\mathrm{g}} r_{\mathrm{b}}} \left(C_{\mathrm{dO}} - K_{\mathrm{O}} p_{\mathrm{g}} \frac{C_{\mathrm{O}}}{C_{\mathrm{O}} + C_{\mathrm{N}}} \right) \tag{33}$$

$$\mathscr{S}_{\mathrm{N}} = \frac{3\mathscr{R} T_{\mathrm{g}}(C_{\mathrm{O}} + C_{\mathrm{N}}) h_{\mathrm{m}}}{p_{\mathrm{g}} r_{\mathrm{b}}} \left(C_{\mathrm{dN}} - K_{\mathrm{N}} p_{\mathrm{g}} \frac{C_{\mathrm{N}}}{C_{\mathrm{O}} + C_{\mathrm{N}}} \right) \tag{34}$$

where the mass transfer coefficient h_{m} is assumed to be the same for both species. It is expressed as a function of the bubble radius, varying linearly between zero (for $r_{\mathrm{b}} = 0$) and 4×10^{-4} m/s (for $r_{\mathrm{b}} = 6.67 \times 10^{-4}$ m) and leveling off at that value for larger bubbles. We refer to Wüest et al. (1992) for further details. Values for Henry's constant at 20 °C are taken as $K_{\mathrm{O}} = 1.3516$ mol m^{-3} bar^{-1} and $K_{\mathrm{N}} = 0.6788$ mol m^{-3} bar^{-1}.

3. Numerical implementation

The numerical implementation of the CFD model is performed with finite elements. Bilinear interpolation is used in the simulations discussed here. The equations are advanced in time decomposing the time step into several substeps, as follows:

1. *Pressure gradient projection:* We are using an equal order formulation stabilized by pressure gradient projection, which has been proposed by Codina and Blasco (1997, 2000) and thoroughly discussed by Buscaglia et al. (2000) and Codina et al. (2001). The first step needed is the orthogonal projection of the pressure gradient onto the velocity interpolation space. This is accomplished using the lumped mass matrix.
2. *Navier–Stokes system:* With the calculated projected pressure gradient and the turbulent viscosity and effective density from the previous time step, the system (17) and (18) is solved with a backward-Euler scheme. The convection term is linearized in the usual way, $\rho_0(u_{\mathrm{m}}^n \cdot \nabla) u_{\mathrm{m}}^{n+1}$. The SUPG method is used as upwinding technique for the convection terms in all substeps.

3. *k–ϵ system:* The standard equations for k and ϵ are solved using the already computed velocity field. The specific implementation, in particular concerning the treatment of spurious negative values of the variables, can be found in the article by Lew et al. (2001).
4. *Bubbles' slip velocity evaluation:* Using (27), with C_O, C_N and N_b from the previous time step, the bubble radius is calculated and the bubbles' slip velocity w_b evaluated at all nodes of the mesh.
5. *Gaseous concentrations variables:* Computing the gas velocity as $u_g = u_m + \mathbf{k}w_b$, the equations for N_b (20), C_O (25) and C_N (26) are advanced in time, with the source terms evaluated at the previous time step. The remaining terms are treated implicitly in time, with one exception: Let f be a gas variable, then, since u_g is not necessarily solenoidal, there appears a term $f \operatorname{div} u_g$. This term is treated either implicitly or explicitly depending on whether $\operatorname{div} u_g$ is positive or negative, respectively; and the condition is applied pointwise through the Gaussian-points do-loop. Significant stability and robustness was gained with this simple trick.
6. *Liquid chemistry variables:* Finally, Eqs. (28)–(30) are advanced in time. Though updated values of C_O, C_N and N_b are available, the sources (33) and (34) are computed with values frozen at the previous time step, so that they are consistent with those used at the previous substep and (31) and (32) hold exactly. This makes the algorithm globally conservative.

4. Integral equations

An integral model is readily obtained from the model introduced before after some definitions and approximations.

Let $S(z)$ be a horizontal surface at distance z from the bottom, with $\mathbf{n}$ the unit upward normal. The horizontal extent of the domain is assumed infinite and the flow is assumed to be in its steady state. Let $m(z)$ be the volumetric flux, $m(z) = \int_{S(z)} u_m \cdot \mathbf{n}\,\mathrm{d}S$, and $M(z)$ the momentum flux, $M(z) = \int_{S(z)} |u_m \cdot \mathbf{n}|^2\,\mathrm{d}S$. From m and M we can *define* a plume width as $b(z) = m(z)/(\pi M)^{1/2}$ and a plume vertical velocity as $w(z) = M/m$. The buoyancy force in the section $S(z)$ is further defined as

$$B(z) = \int_{S(z)} \alpha_g g\,\mathrm{d}S \tag{35}$$

Finally, the volumetric flux per unit length $\mu_e(z)$ entrained by the plume from the surrounding liquid is used to define an entrainment coefficient as $\alpha(z) = \mu_e(z)/(2\pi b(z)w(z))$, so that by integrating (17) over $S(z)$ one gets

$$\frac{\mathrm{d}m}{\mathrm{d}z} = 2\pi\alpha(z)b(z)w(z) \tag{36}$$

This entrainment coefficient turns out to be $\sqrt{2}$ times the usual one.

To obtain the momentum equation it is assumed that the pressure is hydrostatic and that the effect of the turbulent normal stresses can be neglected, yielding

$$\frac{\mathrm{d}M}{\mathrm{d}z} = B(z) \tag{37}$$

This equation uses the approximation

$$\frac{1}{\rho_0}\int_{S(z)}\left(-\frac{\partial\hat{p}_\mathrm{m}}{\partial z}+\rho_0 g+2\frac{\partial}{\partial z}\mu_\mathrm{T}\frac{\partial u_\mathrm{m}\cdot\mathbf{n}}{\partial z}\right)\mathrm{d}S\simeq 0 \tag{38}$$

which relies on neglecting dynamic pressure effects and axial turbulent diffusion of momentum.

Let us now define the molar currents

$$J_\mathrm{O}(z)=\int_{S(z)}(u_\mathrm{m}\cdot\mathbf{n}+w_\mathrm{b})C_\mathrm{O}\,\mathrm{d}S,\quad J_\mathrm{N}(z)=\int_{S(z)}(u_\mathrm{m}\cdot\mathbf{n}+w_\mathrm{b})C_\mathrm{N}\,\mathrm{d}S \tag{39}$$

$$J_\mathrm{dO}(z)=\int_{S(z)}u_\mathrm{m}\cdot\mathbf{n}\,C_\mathrm{dO}\,\mathrm{d}S,\quad J_\mathrm{dN}(z)=\int_{S(z)}u_\mathrm{m}\cdot\mathbf{n}\,C_\mathrm{dN}\,\mathrm{d}S \tag{40}$$

and the entrainment plus integrated source terms

$$Q_\mathrm{O}(z)=\int_{S(z)}\mathscr{S}_\mathrm{O}\,\mathrm{d}S,\quad Q_\mathrm{N}(z)=\int_{S(z)}\mathscr{S}_\mathrm{N}\,\mathrm{d}S \tag{41}$$

$$Q_\mathrm{dO}(z)=\int_{S(z)}\mathscr{S}_\mathrm{dO}\,\mathrm{d}S+2\pi\alpha(z)b(z)w(z)C_\mathrm{dO,a} \tag{42}$$

$$Q_\mathrm{dN}(z)=\int_{S(z)}\mathscr{S}_\mathrm{dN}\,\mathrm{d}S+2\pi\alpha(z)b(z)w(z)C_\mathrm{dN,a} \tag{43}$$

where the subscript a refers to ambient values of the concentrations of dissolved gases (the ambient is assumed to contain no bubbles). Integrating (25), (26), (28) and (29) over $S(z)$, considering steady state flow and neglecting vertical diffusive effects one gets

$$\frac{\mathrm{d}J_\mathrm{O}}{\mathrm{d}z}=Q_\mathrm{O},\quad \frac{\mathrm{d}J_\mathrm{N}}{\mathrm{d}z}=Q_\mathrm{N} \tag{44}$$

$$\frac{\mathrm{d}J_\mathrm{dO}}{\mathrm{d}z}=Q_\mathrm{dO},\quad \frac{\mathrm{d}J_{\mathrm{d}N}}{\mathrm{d}z}=Q_\mathrm{dN} \tag{45}$$

Except for (38), the previous equations are either definitions or exact relations. Now we introduce plume counterparts (underlined) of pointwise quantities, with the following *definitions*:

$$\underline{C_\mathrm{O}}(z)=\frac{J_\mathrm{O}}{\pi\lambda^2 b^2(w+\underline{w_\mathrm{b}})} \tag{46}$$

$$\underline{C_\mathrm{N}}(z)=\frac{J_\mathrm{N}}{\pi\lambda^2 b^2(w+\underline{w_\mathrm{b}})} \tag{47}$$

$$\underline{C_\mathrm{dO}}(z)=\frac{J_\mathrm{dO}}{\pi b^2 w} \tag{48}$$

$$\underline{C_\mathrm{dN}}(z)=\frac{J_\mathrm{dN}}{\pi b^2 w} \tag{49}$$

$$\underline{N_\mathrm{b}}(z)=\frac{\Omega}{\pi\lambda^2 b^2(w+\underline{w_\mathrm{b}})} \tag{50}$$

$$\underline{w_\mathrm{b}}(z)=w_\mathrm{b}(\underline{r_\mathrm{b}}) \tag{51}$$

$$\underline{h_{\mathrm{m}}}(z) = h_{\mathrm{m}}(\underline{r_{\mathrm{b}}}) \tag{52}$$

$$\underline{v_{\mathrm{b}}}(z) = \frac{(\underline{C_{\mathrm{O}}} + \underline{C_{\mathrm{N}}})\mathscr{R}T_{\mathrm{g}}}{p_{\mathrm{g}}\underline{N_{\mathrm{b}}}} \tag{53}$$

$$\underline{r_{\mathrm{b}}}(z) = \left(\frac{3\underline{v_{\mathrm{b}}}}{4\pi}\right)^{1/3} \tag{54}$$

where λ is the ratio of the bubble-core width to the plume width and Ω is the bubble release rate. We assume for simplicity that L is spatially uniform. The integral model keeps the balance (36), (37), (44) and (45), *approximating* the source terms with

$$B(z) \simeq \underline{B}(z) = \pi\lambda^2 b^2 g \underline{N_{\mathrm{b}}}\ \underline{v_{\mathrm{b}}} \tag{55}$$

$$Q_{\mathrm{O}}(z) \simeq \underline{Q_{\mathrm{O}}}(z) = \pi\lambda^2 b^2 \mathscr{S}_{\mathrm{O}}(\underline{C_{\mathrm{O}}}, \underline{C_{\mathrm{N}}}, \underline{C_{\mathrm{dO}}}, \underline{C_{\mathrm{dN}}}, \underline{r_{\mathrm{b}}}, \underline{h_{\mathrm{m}}}) \tag{56}$$

$$Q_{\mathrm{N}}(z) \simeq \underline{Q_{\mathrm{N}}}(z) = \pi\lambda^2 b^2 \mathscr{S}_{\mathrm{N}}(\underline{C_{\mathrm{O}}}, \underline{C_{\mathrm{N}}}, \underline{C_{\mathrm{dO}}}, \underline{C_{\mathrm{dN}}}, \underline{r_{\mathrm{b}}}, \underline{h_{\mathrm{m}}}) \tag{57}$$

$$Q_{\mathrm{dO}}(z) \simeq \underline{Q_{\mathrm{dO}}}(z) = \pi b^2 \mathscr{S}_{\mathrm{dO}}(\underline{C_{\mathrm{O}}}, \underline{C_{\mathrm{N}}}, \underline{C_{\mathrm{dO}}}, \underline{C_{\mathrm{dN}}}, \underline{r_{\mathrm{b}}}, \underline{h_{\mathrm{m}}}) + 2\pi\alpha b w C_{\mathrm{dO,a}} \tag{58}$$

$$Q_{\mathrm{dN}}(z) \simeq \underline{Q_{\mathrm{dN}}}(z) = \pi b^2 \mathscr{S}_{\mathrm{dN}}(\underline{C_{\mathrm{O}}}, \underline{C_{\mathrm{N}}}, \underline{C_{dO}}, \underline{C_{\mathrm{dN}}}, \underline{r_{\mathrm{b}}}, \underline{h_{\mathrm{m}}}) + 2\pi\alpha b w C_{\mathrm{dN,a}} \tag{59}$$

where the exchange terms are defined by (31)–(34) but evaluated with the plume-averaged quantities. The previous approximations provide the *closure* relations to the integral model, supplemented by the assumption that α and λ do not depend on z and can be given empirically based values.

5. Numerical results

5.1. Description of the tests

The simulations reported here are performed at prototype scale, for the case of McCook Reservoir in Chicago, Illinois. For a 100-year storm the water depth in McCook reservoir is expected to be of 77 m. Atmospheric air is injected at the bottom through a circle of diameter 65 cm, with a molar composition of 21% oxygen and 79% nitrogen, at a volumetric rate Q_{g} (at the bottom pressure). Ambient concentrations are 1 mg/l of dissolved oxygen and 0.28 mg/l of dissolved nitrogen. The biochemical oxygen demand is taken as 30 mg/l. Typical conditions are $Q_{\mathrm{g}} = 1.2$ l/s, with a bubble radius of 2.5 mm, but simulations under other conditions have also been performed.

The CFD simulations consider axisymmetric conditions, so that a 2D mesh of 8000 bilinear quadrilaterals is adopted. This mesh is called COARSE mesh, the minimum element sizes are $\Delta r = 14$ mm and $\Delta z = 32$ mm (see Fig. 1). The FINE mesh used in the convergence study is obtained by dividing each quadrilateral into four, so that the grid size is halved.

The domain extends horizontally up to a radius of 100 m, which is large enough for finite-size effects to be negligible (the downwards counterflow at the exterior boundary has a velocity of 0.4 mm/s, less than 0.3% of the plume's velocity). Symmetry conditions were imposed at the artificial vertical boundary. The same was done at the top boundary for the liquid phase, while for the gas

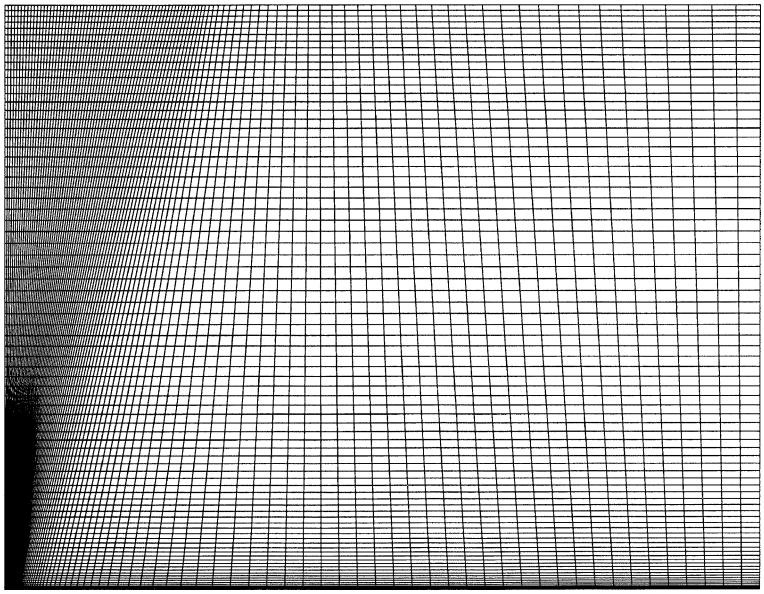

Fig. 1. Mesh used in calculations at reservoir's scale.

phase the top surface is an outflow boundary. The logarithmic smooth-wall law was imposed at the bottom. Since we are analyzing processes in the plume's vicinity, simulations were run for about 3000 s of simulated time (time steps used were in the range 1–4 s), for which all the near-plume variables are stable. The full establishment of the far-field flow for this geometry takes more than 10 times that value, but the plume's quantities discussed here are not affected.

The 1D simulations with the integral model are automatically steady. The Froude number at the plume's origin was adjusted to 1.6, as suggested by Wüest et al. (1992). The empirical coefficients were assigned the values $\alpha = 0.11$ and $\lambda = 0.8$, as recommended by the same authors, except where it is stated otherwise.

5.2. Sample CFD results

Let us briefly overview some sample CFD results at nominal conditions $Q_g = 1.2$ l/s, inlet bubble radius of 2.5 mm. In Fig. 2 the velocity field is depicted. The conical shape of the plume is evident, up to a depth of about 15 m ($z = 52$ m) where the effect of the surface becomes significant and lateral spreading begins. This surface-affected depth (about 25% of total depth) is in agreement with observations by Ditmars and Cederwall (1974).

Fig. 3 depicts some CFD results concerning the gaseous phase. In part (a) of the figure the volume fraction α_g is shown. Practically all the plume has $\alpha_g < 10^{-2}$, a posteriori validating the quasi-incompressibility assumption and the $u_\ell \simeq u_m$ assumption made while deriving the model. Part (b) shows the bubble radius, which is fairly constant throughout the plume because mass transfer effects approximately cancel out with compressibility effects (see Bombardelli et al., submitted for publication). Near the surface, however, compressibility eventually governs the gas density and the bubbles' radius is seen to grow more significantly. In part (c) the molar fraction of

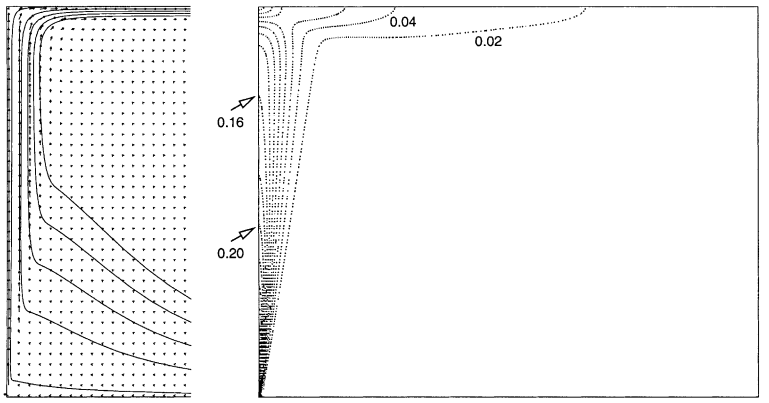

Fig. 2. Velocity field u_m obtained with the CFD code. $Q_g = 1.2$ l/s and $r_b = 2.5$ mm at the inlet. (a) Velocity vectors and a few selected streamlines. (b) Equispaced velocity-modulus contours, contour interval is 0.02 m/s. The maximum of $|u_m|$ over the domain is 0.425 m/s.

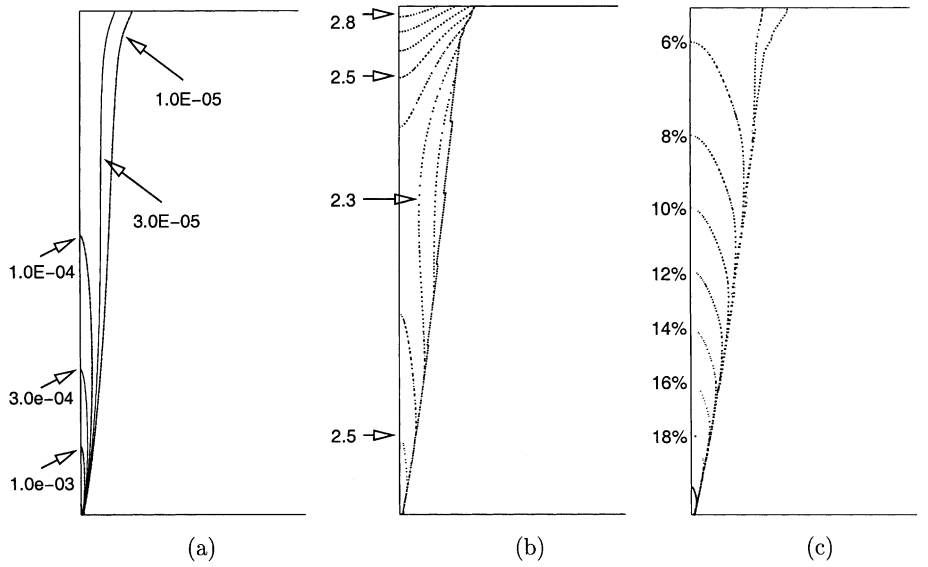

Fig. 3. Results of the CFD code for the gaseous phase variables. (a) Volume fraction α_g. (b) Bubble radius in mm (only calculated where $N_b > 10$ bubbles/m^3). (c) Molar fraction of oxygen in the gas.

oxygen in the bubbles' gas is shown. The simulation predicts that the gas leaving from the surface (which in fact is only 11% of the injected gas) is largely oxygen depleted to about 6%. Notice also the horizontal gradients in the gas composition; this affects the partial pressure of each species inside the bubbles and thus the mass transfer at the interface (see Eqs. (33) and (34)).

To check grid independence of the results a run with the same nominal conditions was run with mesh FINE, which has 200×160 quadrilaterals and half the mesh size of the previous run.

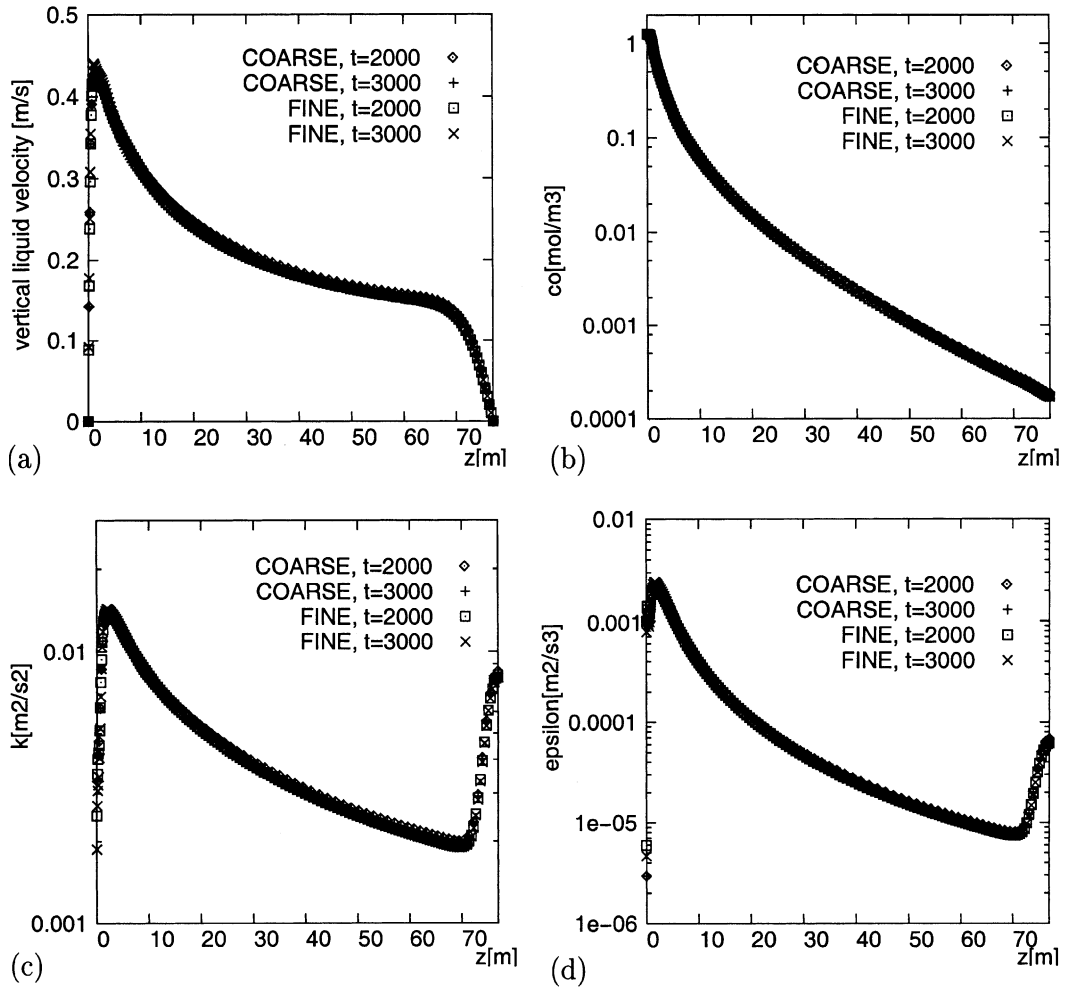

Fig. 4. A comparison of the numerical results obtained using meshes FINE and COARSE, for instants $t = 2000$ s and $t = 3000$ s, so as to check grid independence and steadiness of the solution. We plot, as functions of z, the following variables along centreline: (a) vertical liquid velocity, (b) gaseous oxygen concentration, (c) k, (d) ϵ.

In Fig. 4 we show comparisons of the results obtained with both meshes along the centerline. Not only good agreement is found in the velocity and oxygen concentration, but also in the turbulent variables (k and ϵ). In the same figure the results at $t = 2000$ s are shown, proving the steadiness of the flow variables at the plume.

5.3. Comparison of results of CFD and 1D codes

Most important concerning aeration plumes are global parameters such as the fraction of the injected air that dissolves in the water and the so-called gas holdup, defined as the amount of gas present in the water column at each given instant. For plumes with inlet bubble radius of 2.5 mm

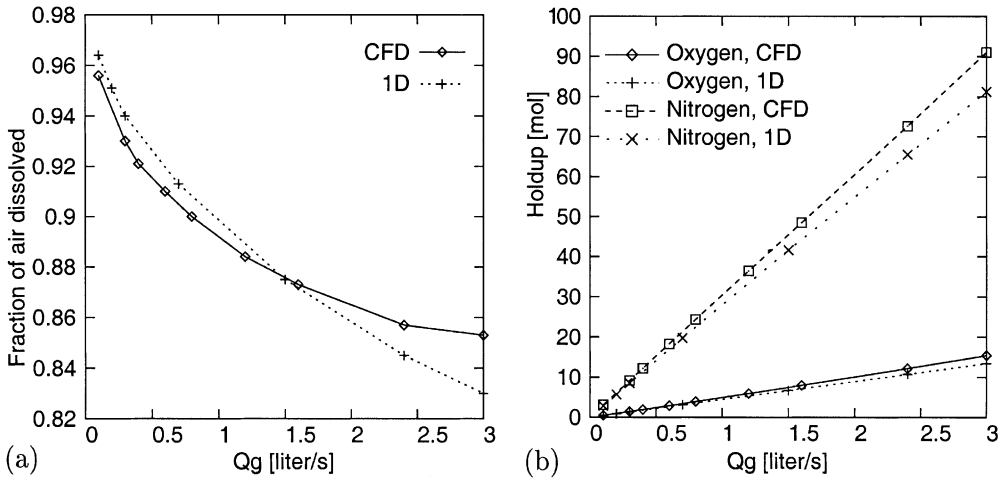

Fig. 5. Comparison of global parameters obtained from the CFD and 1D results. (a) Fraction of the injected gas that dissolves in the plume. (b) Gas holdup, discriminated by species. Both as functions of Q_g.

these quantities are plotted as functions of Q_g in Fig. 5. In part (a) we compare the fraction of air dissolved (FAD) as calculated with the CFD code to that obtained with the 1D model described in Section 4. A quite good agreement is observed over the whole range 0.1–3 l/s. The decrease in FAD with Q_g is due to the smaller residence time of each bubble in the water column, due to the increase in the liquid's velocity with Q_g. This is coherently predicted by both models. For $Q_g > 2$ the FAD in the CFD results tends to level off, while the 1D results keep decreasing with Q_g, but both results differ by less than a few percents so that this discrepancy was not further studied. In part (b) a similar comparison is shown for oxygen and nitrogen holdups, with good agreement.

From the CFD results one can evaluate an equivalent plume liquid's velocity from the definition $w(z) = M(z)/m(z)$. However, since the radial profiles of the vertical component of u_m are almost exactly Gaussian, we use the approximation $w(z) \simeq (1/2)u_m(r = 0, z) \cdot \mathbf{k}$, which is exact for Gaussian velocity profiles. We compare the functions $w(z)$ obtained in this way to those predicted by the 1D model in Fig. 6(a), for $Q_g = 0.3$, 1.2 and 3.0 l/s. The agreement is quite good except in two regions: The first few meters and near the surface. The latter is natural, since w must go to zero at the free surface but this is not accounted for in the 1D model. The discrepancies in the first few meters, on the other hand, are explained by the different flow geometries near the diffuser assumed by the two models. As explained by Wüest et al. (1992) the 1D model imposes an initial Froude number that implies a non-zero liquid mass flow rate *at the diffuser*. This is not modeled by the boundary condition of the CFD run. Bombardelli et al. (submitted for publication) show that this only affects the plume's variables locally, in the first few meters above the diffuser.

In Fig. 6(b) we compare predictions of the CFD and 1D models for bubbles' radius variations with z. The CFD result shown is the bubble-flux-weighted horizontal mean

$$\overline{r_b}(z) = \frac{\int_{S(z)} r_b N_b (u_m \cdot \mathbf{n} + w_b)\, dS}{\int_{S(z)} N_b (u_m \cdot \mathbf{n} + w_b)\, dS}$$

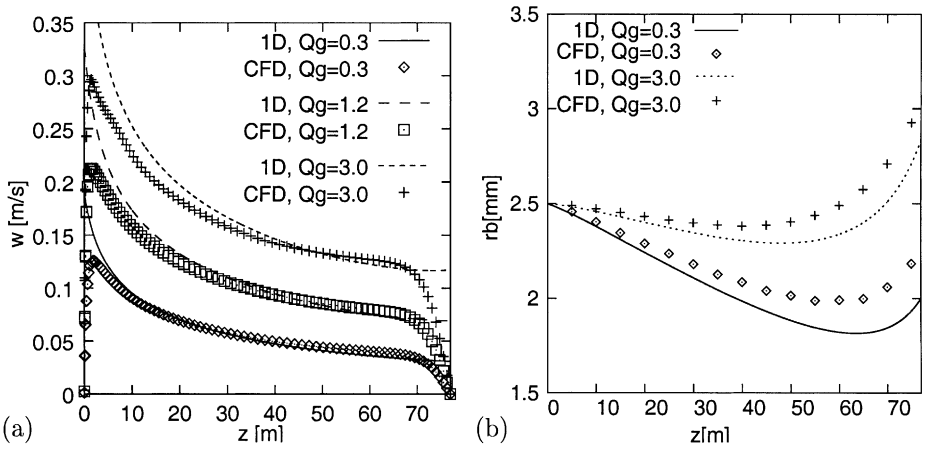

Fig. 6. Comparison of vertical profiles of (a) mean liquid velocity (denoted by w in the text) and (b) mean bubble radius, for several values of Q_g.

The 1D plot simply corresponds to $\underline{r_b}(z)$. One observes that the r_b predicted by the CFD model is larger than that from the 1D model. This difference must be regarded as a discrepancy between the models. However, it is not observed to be larger than 5–10% for the cases analyzed.

5.4. Entrainment coefficient

The entrainment coefficient was evaluated from (36), calculating the plume's volumetric flux, momentum flux, width and velocity according to their definitions (see second paragraph of Section 4). This is shown for a particular case ($Q_g = 1.2$ l/s) in Fig. 7, but the behavior is quite the

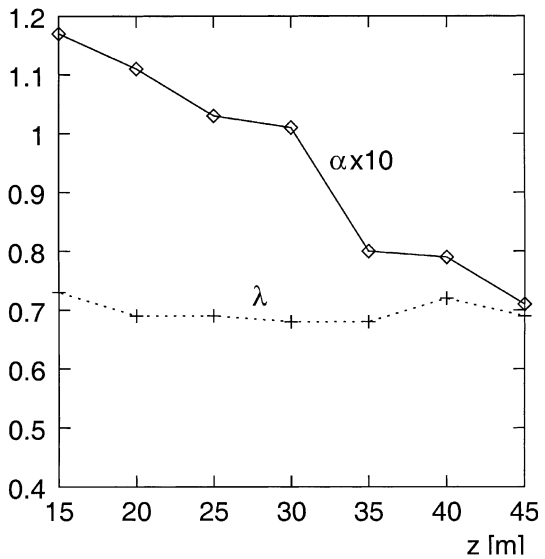

Fig. 7. Values of α and λ as obtained from the CFD results, as functions of z, for the simulation with $Q_g = 1.2$ l/s.

same in all the runs made. The values are of the order of 0.1, decreasing from the diffuser upwards. Notice that the analysis was carried out between $z = 15$ and 45 m, where no effects of the bottom wall or of the free surface is noticeable.

Milgram (1983) obtained quite similar values in his experiments in a 50-m deep reservoir with $Q_g = 4.1$ l/s ($\alpha \simeq 0.085$, after multiplying his values by $\sqrt{2}$ because of a difference in the definition of α). Milgram measured entrainments coefficients that increased with z, contrary to our CFD results, but most of his data are at extremely high gas flow rates. The data of Fannelop & Sjoen as analyzed by Milgram (1983) also exhibit entrainment coefficients that agree with our CFD results. For $Q_g = 2.5$ l/s they obtained $\alpha \simeq 0.1$, increasing up to a $\alpha = 0.14$ for $Q_g = 12$ l/s. Remarkably, their data also show entrainment coefficients that *decrease* with z, particularly for the lower flow rates. Other available values of α also fall in the range 0.07–0.12, such as those of Ditmars and Cederwall (1974) and those of Tekeli and Maxwell (1978). Entrainment coefficients obtained from the CFD code are thus in reasonable agreement with experimental data, notwithstanding the simplicity of the turbulent model employed.

Since the radial profiles of α_g and of the vertical component of u_m are almost exactly Gaussian, it is easy to evaluate $\lambda(z)$ from the CFD results as simply the ratio of the two widths. As shown in Fig. 7, a fairly constant λ of approximately 0.7 is obtained. This is in agreement with the values reported by Milgram (1983) and by Tekeli and Maxwell (1978). Notice that, following the recommendations of Wüest et al. (1992), the 1D code in the previous section was run with $\lambda = 0.8$, while the CFD assessment suggests a value of 0.7. The 1D results depend however very weakly on λ, and changing it from 0.8 to 0.7 would not noticeably affect the results of the previous section. Changes in the holdup, for example, are smaller than 0.1%.

5.5. CFD-based assessment of approximations in 1D model

In Section 4 we have identified the approximations involved in the 1D model. Two of them where addressed before, since they concerned the constancy of α and λ over the depth and the possibility of assigning them empirical values.

We will assess here some of the remaining ones, given by (38), (55) and (56). The rest of the approximations are expected to obey the same behavior. Once more we concentrate on the case $Q_g = 1.2$ l/s, and define the following relative error measures (which are functions of z):

$$E(p) = \frac{\left| \frac{1}{\rho_0} \int_{S(z)} \left(-\frac{\partial \hat{p}_m}{\partial z} + \rho_0 g \right) \mathrm{d}S \right|}{B(z)} \tag{60}$$

$$E(B) = \frac{|B(z) - \underline{B}(z)|}{B(z)} \tag{61}$$

$$E(Q_O) = \frac{|Q_O(z) - \underline{Q_O}(z)|}{|Q_O(z)|} \tag{62}$$

The ratio of dynamic pressure effects and of turbulent vertical transport of momentum to buoyancy is estimated by $E(p)$, while the errors involved in the approximations (55) and (56) are given by $E(B)$ and $E(Q_O)$, respectively. All the quantities appearing in the error measures were

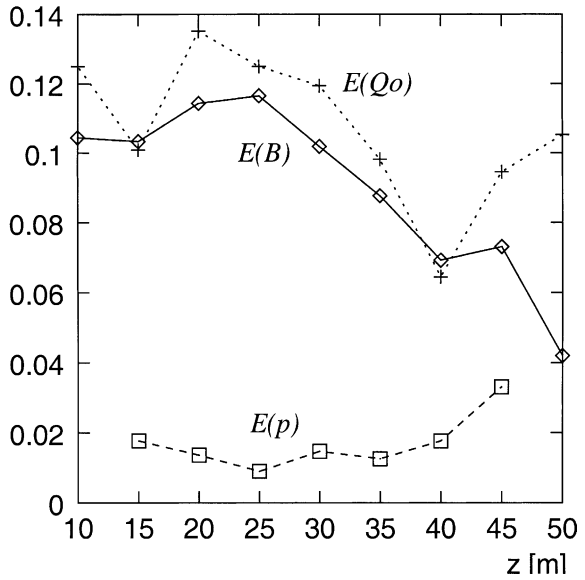

Fig. 8. CFD-based assessment of the approximations made in integral models. Shown are $E(p)$, $E(B)$ and $E(Q_O)$ as functions of z. The definitions can be found in (60)–(62).

calculated from the CFD results following their respective definitions, taking $\lambda = 0.7$. The results of the 1D model for the same case are *not* used at all in this assessment.

In Fig. 8 we show the approximation errors between $z = 10$ m and $z = 50$ m. The dynamic pressure gradient and the turbulent transport of momentum are smaller than 4% of the buoyancy term, so that little or no effect is to be expected from considering them in (37). The approximations (55) and (56) needed as closure of the 1D model, on the other hand, involve errors that are quite homogeneously distributed with z and of about 10%.

6. Conclusions

In this article we have derived a multidimensional mathematical model for dilute bubbly two-phase plumes from the two-fluid model equations. The necessary approximations were discussed and later shown to hold in some cases of interest. The closure relations, in particular concerning Reynolds stresses and turbulent dispersion of the bubbles, were taken from simple models that are reasonable in view of the present knowledge on the subject.

Further on, a mass transfer model was presented that coincides with that of the integral model proposed by Wüest et al. (1992). By coupling this model to the aforementioned two-phase flow model a CFD version of the 1D model was obtained. The derivation of the 1D model from the CFD one was presented in detail and the necessary additional approximations identified.

A set of runs was performed for the conditions of a deep, biochemically active reservoir with a single, isolated plume using both the 1D and CFD codes. By direct comparison good agreement between both models is observed for the most relevant variables such as gas dissolution rates, gas

holdup, liquid's velocity and bubbles' radius. In addition, the entrainment coefficient derived from the CFD results was shown to be consistent with available experimental results. The same was shown for the ratio of the bubbly core width to the plume width. Finally, the approximations inherent in integral models were assessed using the CFD results, proving them to hold within a few percents of relative accuracy.

Our objective has been to present a fully consistent picture of 1D and CFD models for bubble plumes through both mathematical derivation and direct comparison of numerical results. From the good agreement, CFD models can be seen as natural extensions of integral models which have been developed and experimentally verified by the environmental fluid dynamics community over the years. This extension of 1D models to CFD ones is obviously necessary to address many technologically relevant phenomena, such as plume–plume interactions and plumes confined within complex boundaries or immersed in complex crossflows.

We believe that significant understanding of two-phase flow models can be gained by analyzing bubble plumes. Several controversial aspects that were signaled in Section 3 can be assessed by suitably modifying the formulation presented in this paper and selecting appropriate experimental databases for comparison. This is proposed for future work, together with the pending issue of devising a reliable methodology to deal with the suspended solids that are inevitably associated with wastewater resulting from combined-sewer-overflows.

Acknowledgements

The financial support of the U.S. Army Corps of Engineers (Chicago District), through research contract DACA 88-98-D-005-15 is gratefully acknowledged. FAB is on leave from INA, Argentina. GCB is also a fellow of CONICET, Argentina, and received partial support from FOMEC, Argentina. Our thanks are also due to R. Lahey, F. Moraga, R. Codina, A. Larreteguy and P. Carrica for useful discussions.

References

Asaeda, T., Imberger, J., 1993. Structure of bubble plumes in linearly stratified environments. J. Fluid Mech. 249, 35–57.

Ashton, G., 1978. Numerical simulation of air bubbler systems. Can. J. Civ. Eng. 5, 231–238.

Becker, S., Sokolichin, A., Eigenberger, G., 1994. Gas–liquid flow in bubble columns and loop reactors: Part II. Comparison of detailed experiments and flow simulations. Chem. Eng. Sci. 49, 5747–5762.

Besnard, D., Harlow, F., 1988. Turbulence in multiphase flow. Int. J. Multiphase Flow 14, 679–699.

Bombardelli, F., Buscaglia, G., Rehmann, C., García, M. Scaling procedures for aeration bubble plumes, submitted for publication.

Borchers, O., Busch, C., Sokolichin, A., Eigenberger, G., 1999. Applicability of the standard k–ϵ turbulence model to the dynamic simulation of bubble columns: Part II. Comparison of detailed experiments and flow simulations. Chem. Eng. Sci. 54, 5927–5935.

Bulson, P., 1968. The theory and design of bubble breakwaters. In: Proc. 11th Conf. Coastal Engng., London, pp. 995–1015.

Buscaglia, G., Basombrío, F., Codina, R., 2000. Fourier analysis of an equal-order incompressible flow solver stabilized by pressure-gradient projection. Int. J. Numer. Meth. Fluids 34, 65–92.

Carrica, P., Bonetto, F., Drew, D., Lahey Jr., R., 1998. The interaction of background ocean air bubbles with a surface ship. Int. J. Numer. Meth. Fluids 28, 571–600.

Carrica, P., Drew, D., Bonetto, F., Lahey Jr., R., 1999. A polydisperse model for bubbly two-phase flow around a surface ship. Int. J. Multiphase Flow 25, 257–305.

Chapra, S., 1997. Surface Water-Quality Modeling. McGraw-Hill.

Clift, R., Grace, J., Weber, M., 1978. Bubbles, Drops and Particles. Academic Press.

Codina, R., Blasco, J., 1997. A finite element formulation for the Stokes problem allowing equal velocity–pressure interpolation. Comp. Meth. Appl. Mech. Eng. 143, 373–391.

Codina, R., Blasco, J., 2000. Stabilized finite element method for the transient Navier–Stokes equations based on a pressure gradient projection. Comp. Meth. Appl. Mech. Eng. 182, 277–300.

Codina, R., Blasco, J., Buscaglia, G., Huerta, A., 2001. Implementation of a stabilized finite element formulation for the incompressible Navier–Stokes equations based on a pressure gradient projection. Int. J. Numer. Meth. Fluids 37, 410–444.

Ditmars, J., Cederwall, K., 1974. Analysis of air-bubble plumes. In: Proc. 14th Coastal Eng. Conf., Copenhagen. ASCE, pp. 2209–2226.

Drew, D., Passman, S., 1998. Theory of Multicomponent Fluids Applied Mathematical Sciences, vol. 135. Springer.

Druzhinin, O., Elghobashi, S., 1998. Direct numerical simulations of bubble-laden turbulent flows using the two-fluid formulation. Phys. Fluids 10, 685–697.

Ganesan, S., Poirier, D.R., 1990. Conservation of mass and momentum for the flow of inter-dendritic liquid during solidification. Metall. Trans. 21B, 173–181.

Grevet, J., Szekely, J., El-Kaddah, N., 1982. An experimental and theoretical study of gas bubble driven circulation systems. Int. J. Heat Mass Transfer 25, 487–497.

Haberman, W., Morton, R., 1954. An experimental study of bubbles moving in liquids. Proc. Am. Soc. Civ. Eng. 80, 379–427.

Hinze, J., 1955. Fundamentals of the hydrodynamic mechanism of splitting in dispersion processes. AIChE. J. 1, 289–294.

Hua, J., Wang, C.-H., 2000. Numerical simulation of bubble-driven liquid flows. Chem. Eng. Sci. 55, 4159–4173.

Joo, S., Guthrie, R., 1992. Modeling flows and mixing in steelmaking ladles designed for single- and dual-plug bubbling operations. Metall. Trans. B 13B, 765–778.

Kunz, R., Siebert, B., Cope, W., Foster, N., Antal, S., Ettorre, S., 1998. A coupled phasic exchange algorithm for three-dimensional multi-field analysis of heated flows with mass transfer. Comput. Fluids 7, 741–768.

Lemckert, Ch., Imberger, J., 1993. Energetic bubble plumes in arbitrary stratification. J. Hydraul. Eng. 119, 680–703.

Lew, A.J., Buscaglia, G.C., Carrica, P.M., 2001. A note on the numerical treatment of the k–ϵ turbulence model. Int. J. Comput. Fluid Dyn. 14, 201–209.

López de Bertodano, M., 1998. Two fluid model for two-phase turbulent jets. Nucl. Eng. Des. 179, 65–74.

Loth, E., 2000. Numerical approaches for motion of dispersed particles, droplets and bubbles. Progress Energy Combust. Sci. 26, 161–223.

Loth, E., 2001. An Eulerian turbulent diffusion model for particles and bubbles. Int. J. Multiphase Flow 27, 1051–1063.

Malin, M., Spalding, D., 1984. A two-fluid model of turbulence and its application to heated plane jets and wakes. PCH Phys. Chem. Hydrodyn. 5, 339–362.

McDougall, T., 1978. Bubble plumes in stratified environments. J. Fluid Mech. 85, 655–672.

Milgram, J., 1983. Mean flow in round bubble plumes. J. Fluid Mech. 133, 345–376.

Millies, M., Drew, D., Lahey, R., 1996. A first order relaxation model for the prediction of the local interfacial area density in two-phase flows. Int. J. Multiphase Flow 22, 1073–1104.

Millies, M., Mewes, D., 1999. Interfacial area density in bubbly flow. Chem. Eng. Process. 38, 307–319.

Moraga, F., Larreteguy, A., Drew, D., Lahey Jr., R. Assessment of turbulent dispersion models for bubbly flows, submitted for publication.

Morchain, J., Maranges, C., Fonade, C., 2000. CFD modelling of a two-phase jet aerator under influence of a crossflow. Water Res. 34, 3460–3472.

Mudde, R., Simonin, O., 1999. Two- and three-dimensional simulations of a bubble plume using a two-fluid model. Chem. Eng. Sci. 54, 5061–5069.

Ni, J., Beckermann, C., 1991. Volume-averaged two-phase model for transport phenomena during solidification. Metall. Trans. B 22B, 349–361.

Joint Task Force of the Water Pollution Control Federation and the American Society of Civil Engineers, editors, 1988. Aeration: A waste-water treatment process. ASCE—Manuals and Reports on Eng. Practice No. 68. WPCF—ASCE.

Pfleger, D., Gomes, S., Gilbert, N., Wagner, H., 1999. Hydrodynamic simulations of laboratory scale bubble columns fundamental studies of the Eulerian–Eulerian modeling approach. Chem. Eng. Sci. 54, 5091–5099.

Sato, Y., Sadatomi, M., Sekoguchi, K., 1981. Momentum and heat transfer in two-phase bubble flow—I. Int. J. Multiphase Flow 7, 167–177.

Schladow, S., 1992. Bubble plume dynamics in a stratified medium and the implications for water quality amelioration in lakes. Water Resour. Res. 28, 313–321.

Simonin, O., Viollet, P., 1988. On the computation of turbulent two-phase flows in the Eulerian formulation. EUROMECH, 234.

Smith, B., 1998. On the modelling of bubble plumes in a liquid pool. Appl. Math. Modell. 22, 773–797.

Sokolichin, A., Eigenberger, G., 1999. Applicability of the standard k–ϵ turbulence model to the dynamic simulation of bubble columns: Part I. Detailed numerical simulations. Chem. Eng. Sci. 54, 2273–2284.

Song, J., Ishii, M., 2001. On the stability of a one-dimensional two-fluid model. Nucl. Eng. Des. 204, 101–115.

Soo, S.L., 1990. Multiphase Fluid Dynamics. Science Press.

Stock, D., 1996. Particle dispersion in flowing gases. ASME J. Fluids Eng. 118, 4–17.

Taylor, G., 1955. The action of a surface current used as a breakwater. Proc. Roy. Soc. A 231, 466–478.

Tekeli, S., Maxwell, W., 1978. Behavior of air bubble screens. Civil Eng. Studies, Hydraulic Eng. Res. Series 33, University of Illinois at Urbana-Champaign.

Turner, J., 1986. Turbulent entrainment: the development of the entrainment assumption, and its application to geophysical flows. J. Fluid Mech. 173, 431–471.

Viollet, P., Simonin, O., 1994. Modelling dispersed two-phase flows: closure, validation and software development. Appl. Mech. Rev. 47, 80–84.

Wang, L., Stock, D., 1993. Dispersion of heavy particles by turbulent motion. J. Atmos. Sci. 50, 1897–1913.

Wells, M., Stock, D., 1983. The effect of crossing trajectories on the dispersion of particles in a turbulent flow. J. Fluid Mech. 136, 31–62.

Wilcox, D., 1998. Turbulence Modeling for CFD. DCW Industries, La Cañada, California.

Woo, J., Szekely, J., Castillejos, A., Brimacombe, J., 1990. A study on the mathematical modeling of turbulent recirculating flows in gas-stirred ladles. Metall. Trans. B 21B, 269–277.

Wüest, A., Brooks, N., Imboden, D., 1992. Bubble plume modeling for lake restoration. Water Resour. Res. 28, 3235–3250.